ANALYSIS OF THERMO-MECHANICAL BEHAVIOR IN BILLET CASTING

Joong Kil PARK [1], Chunsheng LI [2], Brian G. THOMAS [2] and Indira V. SAMARASEKERA [3]

[1]POSCO, Steelmaking Research Group, Technical Research Lab., Pohang, Kyungbuk, Korea
[2]Department of Mechanical and Industrial Engineering, University of Illinois at Urbana-Champaign, 1206 W Green Street, Urbana, IL, 61801, USA; Tel: 1-217-333-6919 Fax: 1-217-244-6534 Email: bgthomas@uiuc.edu
[3]Department of Metals and Metallurgical Engineering, University of British Columbia, 111-2355 East Mall, Vancouver, BC, Canada

Key Words: Longitudinal Corner Cracks, Bulging, Corner Radius, High-Speed Casting, Finite-Element Simulation.

INTRODUCTION

As the demand for higher quality steel at higher productivity continues to increase, there is a growing need to understand the cause of defects in the continuous casting process and to optimize the casting conditions to avoid them. Longitudinal cracks form at or near the corners of the billet and initiate in or just below the mold. Local thinning of the shell near the corner regions is also observed. In extreme cases, the shell may become so thin that a breakout occurs. Although the mechanism(s) are not fully understood, these problems are worse at higher casting speeds, where the ferrostatic pressure below mold exit causes bulging of the thin shell. In fact, longitudinal cracks impose one of the limits to increasing casting speed.

Two decades of operating experience have shown that reducing the corner radius from 12-16mm down to 3 or 4mm is beneficial in reducing longitudinal corner cracks.[1] In addition to lessening crack frequency, decreasing the corner radius also tends to move the crack location from the corner itself to the off-corner region. Unfortunately, billets with sharp edges tend to "fold over" during the rolling process.[2] Therefore, mold designers must struggle to satisfy these two conflicting requirements. It would be very desirable to find a better way to solve the longitudinal corner crack problems.

As a step towards improving understanding of the cracking mechanisms, and predicting the theoretical limits to casting speed, this work applies finite-element models to compute the thermo-mechanical state of the solidifying shell during continuous casting of steel in a square billet-casting mold. Two different models, AMEC2D and CON2D, are applied to simulate temperature, bulging displacement, stress, and strain in the solidifying shell, and to predict damage leading to crack formation. In the mold, the intermittent air gap between the casting mold and the solidifying strand is also predicted.

This paper first presents examples of the extensive validation of the models, featuring comparison with many different types of plant measurements on the same typical billet casting conditions. The models are next applied to understand how two different types of longitudinal cracks form in steel billets. Then, a parametric study is performed to investigate the effects of important casting parameters on these defects, and to recommend

operating practices to avoid them, including a critical casting speed, as a function of section size and mold length.

PREVIOUS STUDIES ON LONGITUDINAL CRACKS

Longitudinal cracks are one of the most common mold-related quality problems encountered in billet casting. They are related to hot tearing close to the solidification front.[3] They are manifested in at least two different forms: "longitudinal corner cracks" and "off-corner internal cracks".

Longitudinal corner cracks run along the surface near the exact corner of the billet and are usually 1 to 2mm deep[4] as pictured in Fig. 1(a). Although several studies suggest that longitudinal corner cracks are related to the rhomboid condition of the billet [4-8] these cracks also occur in the absence of rhomboidity, due to improper corner radius [4, 9] or mold distortion and wear.[5, 6] Aketa and Ushijima[9] observed that with a large corner radius, the longitudinal corner cracks appear along the corner, while with smaller radii, these surface cracks form more frequently at the off corner region. They suggest that the optimal corner radius to minimize longitudinal crack formation should be 1/10 of the section size.[3] However, Samarasekera [4] believes that the modern trend of smaller corner radii such as 3 or 4mm may solve the longitudinal corner cracking problem, but at the expense of creating more off-corner cracks. Mori[6] observed that the incidence of longitudinal corner cracks increases with the time a mold is in service during a campaign. He suggests that overall reverse of taper may be an important contributor. This was attributed to permanent creep distortion of the upper mold toward the steel and wear in the lower mold with longer service time.
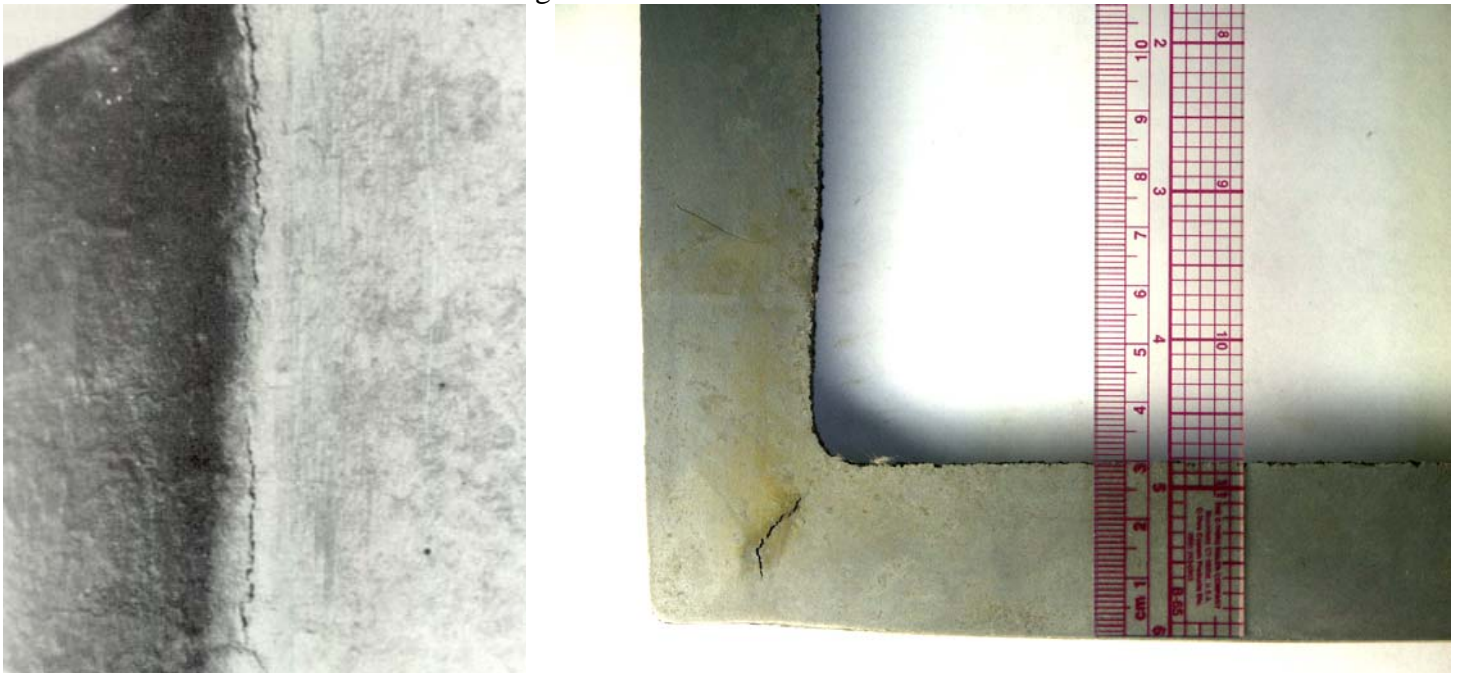
(a) Longitudinal corner crack[4]   (b) Off-corner internal crack

Fig. 1: Appearance of longitudinal cracks in billet casting

Although longitudinal corner cracks are believed to form in the mold[2, 3] off-corner internal cracks are believed to form below the mold in the spray-cooling zone.[10] A typical crack is pictured in the breakout shell in Fig. 1(b).[11] These cracks are typically observed about 15mm from a given corner starting at a depth of 4 to 11mm from the billet surface and extending to a depth of 13-20mm.[4, 10, 12] By analyzing the microstructure of the billet obtained from industrial trials using heat flow calculations, J.K. Brimacombe et al.[10] deduced that cracks can form due to bulging of the solid shell in the lower part of the mold. They propose that as bulging occurs, a hinging action develops near the cold and strong corners, causing off-corner tensile stresses near the solidification front and cracking. The cause of the shell bulging was guessed to be thermal distortion or wear in

the lower region of the mold. This bulging could arise if improperly set foot rolls or wobbling of the mold during its oscillation cycle caused the strand to move about in the lower region of the mold.

MODEL DESCRIPTION

In this study, the transient, thermal-elastic-visco-plastic finite element models, AMEC2D[13, 14] and CON2D[15, 16], are applied to simulate temperature, stress, strain and deformation of a 2-D section of a continuous cast steel billet, as it moves at the casting speed down the mold and below. The detailed formulation of each model is provided elsewhere, so only a brief description is given here. Invoking symmetry, each model domain is one quarter of a 2-D transverse section through the billet, such as pictured in Fig. 2(a), of the CON2D L-shaped domain, which saves computation by leaving out some of the internal liquid. The heat and force balance equations are each solved on a fixed grid of finite elements, such as pictured in Fig. 2(b) of the mesh of 4-node rectangles used in AMEC2D. Each program includes separate finite element models of heat transfer and stress generation that are step-wise coupled through the size and properties of the interfacial gap. Stresses arise primarily due to thermal strains, while heat transfer across the gap depends on the amount of shrinkage of the solidifying shell. During each step of the analysis, the temperature fields of the mold and strand are calculated simultaneously, extrapolating from the previous step, neglecting axial conduction. Then, the stress analysis calculates deformation of the strand, stress and the air gap size. Iteration continues until the heat transfer coefficient calculated from calculated gap is converged.
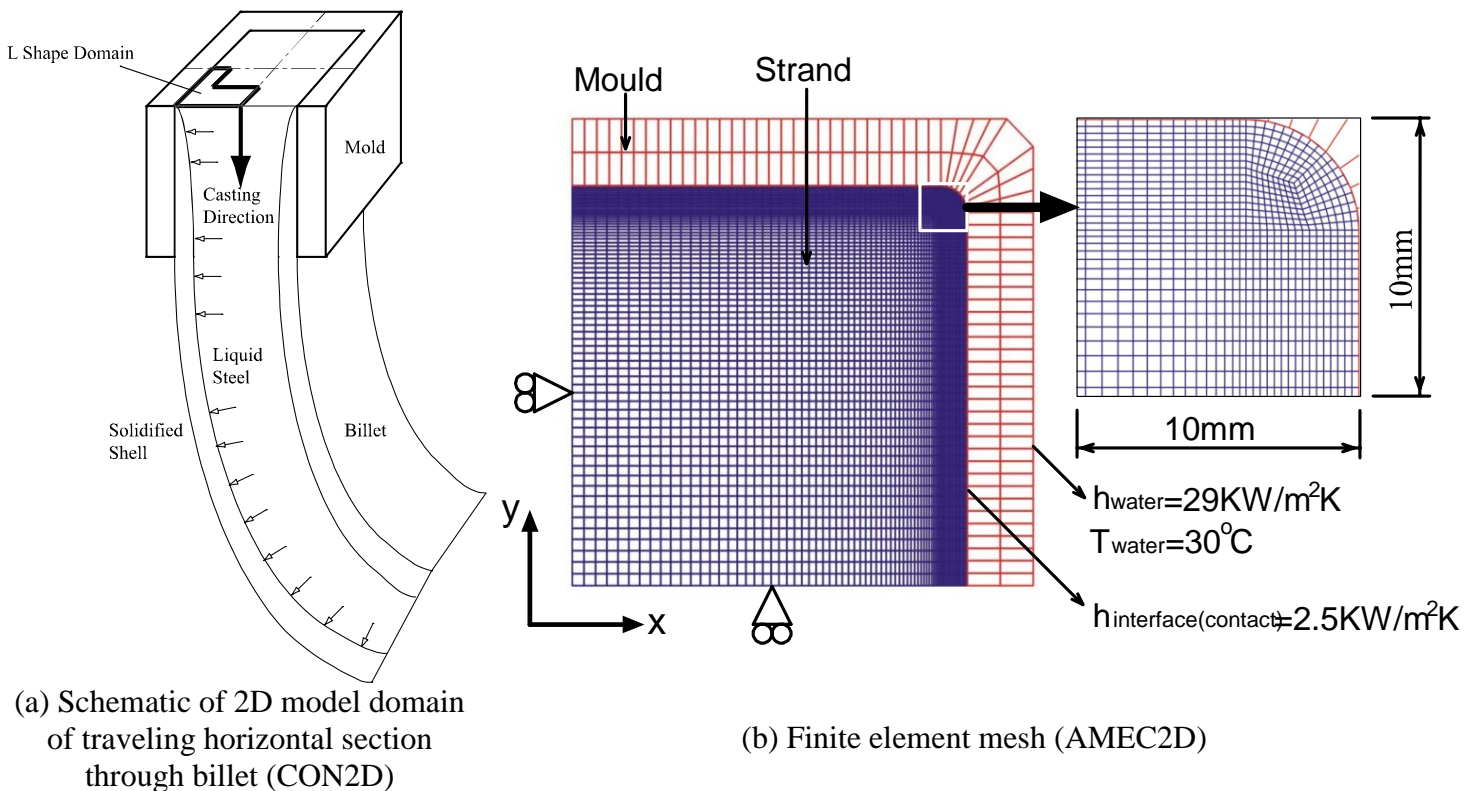

(a) Schematic of 2D model domain
of traveling horizontal section
through billet (CON2D)

(b) Finite element mesh (AMEC2D)

h_{water}=29KW/m^{2}K
T_{water}=30°C

$h_{interface(contact)}$=2.5KW/m^{2}K

Fig. 2: Modeling domain

Heat Transfer Model

The heat transfer model solves the 2D transient conduction equation, using a fixed Lagrangian grid of 3-node triangles (CON2D) or 4-node rectangles (AMEC2D). Latent heat is evaluated using the spatial averaging technique suggested by Lemmon[17]. Axial heat conduction is ignored. A non-equilibrium phase transformation model for plain carbon steels[18] is incorporated to produce realistic phase fraction evolution between solidus

and liquidus temperatures. Further model details, including the composition and temperature-dependent thermal conductivity and enthalpy functions, are given elsewhere for AMEC2D[14] and CON2D[11].

For the plant validation case, the instantaneous interfacial heat flux profile down the mold is found from thermocouple measurements in the mold. The profile is then integrated to find the average heat flux in the mold, which should match a global heat balance with the cooling water. Heat transfer between the shell and mold is governed by a heat transfer coefficient, which varies with position around the mold perimeter and time.

In the parametric study to investigate casting speed, the instantaneous heat flux profile down the mold is assumed to be a function of time:

$$q\left(MW/m^2\right) = \begin{cases} 5 - 0.2444t\,(\text{sec.}) & t \le 1.0\,\text{sec.} \\ 4.7556t\,(\text{sec.})^{-0.504} & t > 1.0\,\text{sec.} \end{cases} \tag{1}$$

This function was obtained by differentiating a curve fitted from the average heat flux data measured by many investigators[19-24], shown in Fig. 3. Slab caster data with mold flux is seen to be lower than billet casting with oil lubrication. Thus, this function is on the low side of billet measurements. This instantaneous heat flux is assumed to be uniform around the perimeter of the billet surface. This corresponds to the assumptions of ideal taper and perfect contact between the shell and mold. Below mold exit, the billet surface temperature is kept unchanged from its circumferential profile at mold exit.
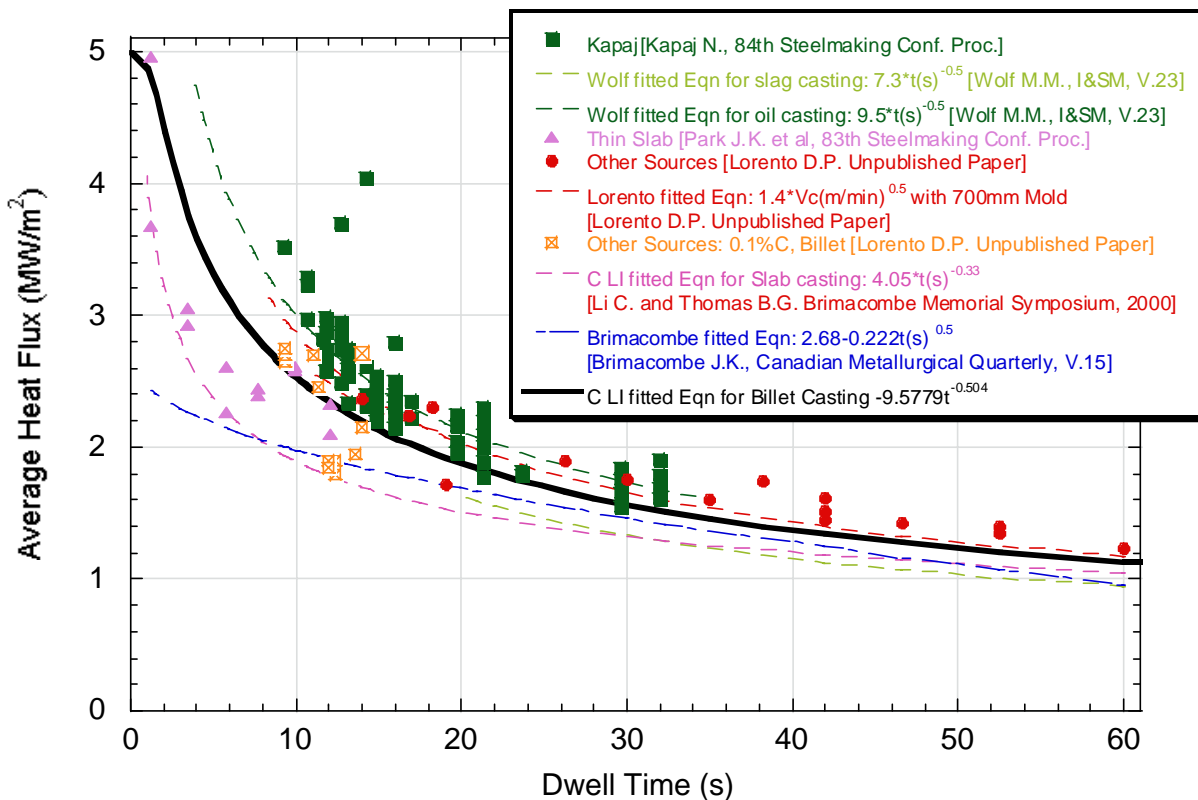

Fig. 3: Measured average mold heat flux and fitted curve used in critical casting speed study

Stress Model

The stress models feature elastic-viscoplastic creep constitutive equations that account for the different mechanical responses of the liquid, semi-solid, delta-ferrite, and austenite phases in addition to the important effects of temperature and strain rate. For example, the ferrite phase creeps faster than austenite at the same temperature and stress level. Temperature and composition-dependent functions are also employed for

important properties, such as thermal linear expansion. Special computational measures are needed to handle the ensure that portions of the domain in the liquid phase are able to transmit ferrostatic pressure while not generating internal shear stresses. A contact algorithm is used to prevent penetration of the shell into the mold wall due to the internal ferrostatic pressure from the head of molten steel. Iteration is needed within each time step to converge on a solution to these highly non-linear equations. Further details are provided elsewhere for AMEC2D[13, 14] and CON2D.[25]

Failure Criteria

Two different failure criteria were used in the present work, in order to predict crack defects that limit casting speed. The first was a bulging criterion, chosen to be a maximum outward displacement (found at the billet centerline) of 1mm, relative to the corner of the billet section. Secondly, a hot tear crack criterion was adopted:

$$\varepsilon_c = \frac{0.02821}{\dot{\varepsilon}^{0.3131} \Delta T_B^{0.8638}} \tag{2}$$

This simple empirical function for the critical strain, ε_c, was fitted by WON[26] from many measurements. It depends on the strain rate, $\dot{\varepsilon}$, which is the average inelastic strain rate within the brittle temperature range, ΔT_B, defined between solid fractions of 90% and 99%. Hot tear cracks form if the thick dendrites in the brittle temperature range prevent the surrounding liquid from feeding to compensate the contraction of interdendritic liquid and solid expansion. The model accumulates "damage strain" by summing the inelastic "flow strain" (caused by the flow of liquid to feed the mushy zone) during time steps when the nodal temperature is within ΔT_B. The critical damage strain component chosen for comparison is taken perpendicular to the dendrite growth direction, which is along the "hoop" direction, tangential to the closest surface of the solidifying shell (x or y face). Cracks are predicted when this damage strain exceeds ε_c. This allows the model to quantify the timing, location and orientation of hot tear cracks.

MODEL VALIDATION

The models are validated both with an analytical solution of thermal stress in a solidifying slab and through comparison with the results of plant trials, including measurements of mold temperature, cooling water temperature rise, shell thickness profiles both down the mold and around the perimeter, and the location of cracks in an etched steel section.

Analytical Solution

The internal consistency of the finite-element models were first validated with the analytical solution of Weiner and Boley[27] for thermal stress during one-dimensional solidification of a semi-infinite plate. The elastic-perfectly plastic yield stress drops linearly with temperature from 20MPa at the surface (held at 1300°C) to 0 MPa at the solidification front (1469°C) with no superheat. Table 1 shows the other conditions for this test problem. The temperature predictions of both models agree well with each other and with the analytical solution at all times, as shown in Fig. 4(a).

Table 1: Constants used in Boley and Weiner analytical solution

Conductivity (W/mK)	33.
Specific Heat (kJ/m³K)	0.70
Latent Heat (kJ/kg)	272.
Elastic Modulus in Solid (GPa)	40.
Elastic Modulus in Liquid (GPa)	14.
Thermal Linear Expansion Coefficient (1/K)	0.00002
Density (kg/m³)	7400.
Poisson's Ratio	0.35
Liquidus Temperature (°C)	1469.
Solidus Temperature (°C)	1468.

Figure 4(b) compares typical stress profiles through the shell thickness. The CON2D computations match within 2% average error with the same mesh and time step sizes used in the actual 2-D analyses in Table 1. This demonstrates that the model is numerically consistent and has an acceptable mesh. The AMEC2D stress results differ, however, due to the assumption of plane strain in AMEC2D, which is different from the true state of generalized plane strain. However, they do agree with CON2D model results for the same stress state, which again implies that the mesh size is adequate.

(a)

(b)
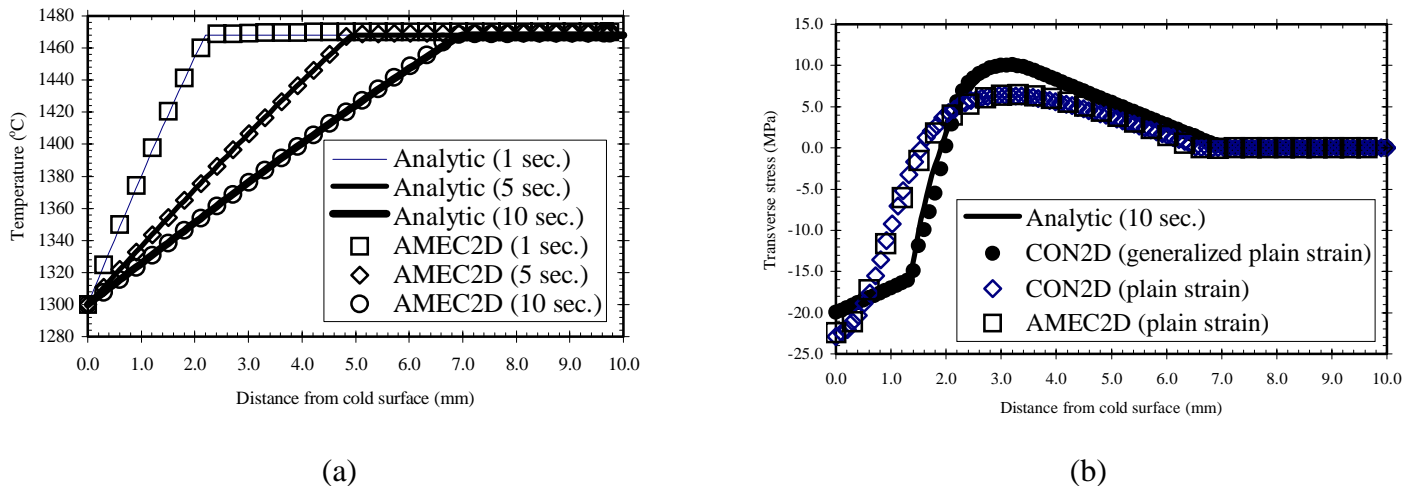
Fig. 4: Comparison of analytical and calculated solution of (a) Temperature and (b) Stress

Plant Trial

A plant trial was conducted at POSCO, Pohang works, South Korea, for a 120mm square section billet of 0.04% C steel continuously cast at 2.2m/min with oil lubrication, open pouring and electromagnetic stirring. The mold tube was relatively pure DHP copper with a wall thickness of 6mm, a corner radius of 4mm and a single linear taper of 0.75%/m. Other operating conditions are provided in Tables 2 and 3.

Table 2: Steels modeled		
	Plant Validation	Speed Study
Steel Composition (wt%)	0.04C, 0.25Mn, 0.2Si, 0.015S, 0.01P	0.27C, 1.52Mn, 0.34Si, 0.015S, 0.012P
Liquidus Temp. (^{o}C)	1529	1501
70% Solid Temp. (^{o}C)	1524	1477
90% Solid Temp. (^{o}C)	1517	1460
Solidus Temp. (^{o}C)	1511	1412

Table 3: Plant validation conditions	
Billet Section Size	120mm×120mm
Total Mold Length	800mm
Meniscus level	100mm
Pouring Temperature	1554 ^{o}C
Casting speed	2.2 m/min
Narrow Face Taper	0.75 %/m
Oscillation stroke	8mm sinusoidal
Lubrication	oil; open pouring
Water velocity	9.2 m/sec.
Water flow rate	1100 l/min.

Mold Temperature Measurement - The mold tube was instrumented with 12 K-type thermocouples on the inside-radius face as shown in Fig. 2(b). They were arranged in three columns along the centerline, and ±45mm from the centerline, and in four rows located at 120mm, 170mm, 400mm and 700mm below the top of the 800mm long mold. The thermocouples were embedded in the mold wall to a depth of 3mm from the hot face. The mold water temperature increase was not recorded at the time, but is estimated to be 30oC based on recent measurements for the same conditions.

Axial mold - temperature profiles were calculated using both models. Figure 5 compares the predictions with the measured mold temperature profile down the mold, found by averaging the thermocouple values across each of the four rows. The heat flux profile in the CON1D model was adjusted carefully in order to match the

temperatures accurately. The AMEC2D model ignores axial heat conduction so is not expected to exactly match, but still agrees reasonably well.[14] Figure 5 also includes the hot and cold face temperature.

The corresponding heat flux profiles predicted by both models are compared in Fig. 6. The accurate CON1D model curve shows a slight dip and rebound in heat flux somewhere from 20 – 100mm below the meniscus. This is due to the unexpected lower temperature measured by the highest thermocouple. It is interesting to note that this drop corresponds roughly with the region of negative mold distortion, suggesting that this negative taper at the meniscus might play a role. This heat-flux dip phenomenon has been observed by others in billet molds.[12, 28, 29] The AMEC2D curve is the classic monotonically decreasing profile, which is more commonly observed.
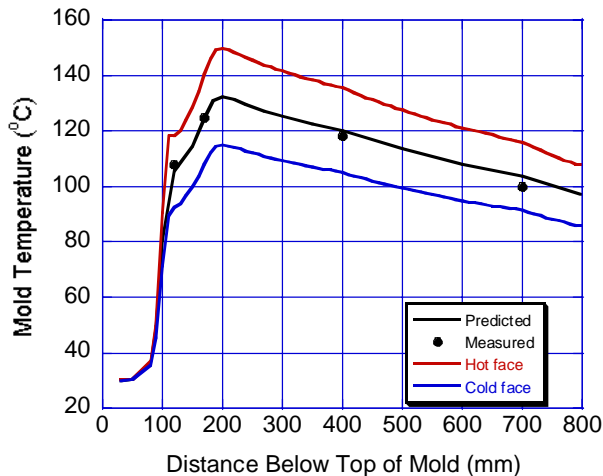
Fig. 5: Comparison of measured and calculated (CON1D) mold temperatures
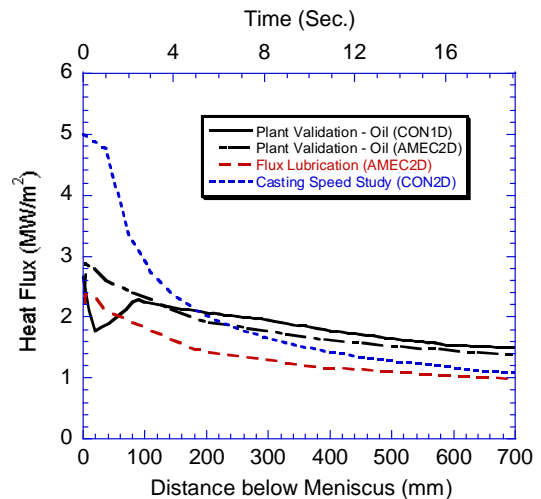
Fig. 6: Heat flux profiles used in model simulations

Heat flux for the mold power casting case is also included in Fig. 6. Its overall heat flux is much lower than the oil casting case. This result agrees with other work.[30] This lower heat flux is due to the insulating effect of the mold flux layer between the mold and strand. Figure 6 includes the heat flux curve used in the CON2D study to investigate critical casting speed, based on the measurements in Fig. 3. This shows that the plant validation measurements are typical of measurements elsewhere, except perhaps being slightly low near the meniscus.

Heat Balance - To validate the heat flux profiles, a comparison was made with an energy balance performed on the cooling water. The model predictions of average heat flux, found from the area under the curves in Fig. 6, are 1.84 and 1.80 MW/m^2 for CON1D and AMEC2D respectively. The measured cooling-water temperature increase of 8 ^{o}C corresponds to an average heat flux of 1.84MW/m^2, which agrees quite well with both of the model predictions.

Solid Shell Thickness Measurement - To investigate the solid shell growth, FeS tracer was suddenly added into the liquid pool during steady state casting. Because FeS cannot penetrate the solid shell, the position of the solid shell front at that instant can be clearly recognized after casting using a sulfur print.

Figure 7 compares the measured solid shell thickness in a transverse section through the billet with the corresponding model prediction. The transverse section was taken at 285mm below the meniscus, which corresponds to a simulation time of 7.8 second. The deformed shape of the strand is superimposed with temperature contours in the same figure. Shell thickness was defined in the model as the isotherm corresponding to the coherency temperature, assumed to be 70% solid. The general shapes of the predicted and measured solid shell match quite reasonably. It is noted that the model also can predict the re-entrant corner

effect that is observed in the sulfur print. This agreement appears to validate the remaining features of this model, including the air gap formation in the corner region.

The shell thickness was plotted in Fig. 8 as a function of residence time in the mold. Also plotted in the figure are the plant trial measurements by tracer test. As seen in Fig. 8, the predicted solid shell growth is quite reasonable, considering the uncertainty about the penetration depth of the tracer into the mushy zone of the solidifying shell.

Bulging Below the Mold - The strand shell exiting the mold is weak and hot, so the internal liquid pressure bulges the shell outward below the mold. The amount of bulging depends on the temperature and strength of the shell at mold exit. Although it might be supposed that bulging in billet casting is small compared with slab casting, the higher casting speeds and lack of support can make it significant. This bulging can cause internal strain in the shell, depending on billet geometry features such as corner radius and taper.

Figure 9 shows the evolution of displacement at the center and corner of the billet surface. The predicted bulging at the center of billet is shown to be about 1.4mm, with respect to the displacement of the billet corner. The bulging of the billet cast during

Fig. 7: Comparison of measured and calculated (AMEC2D) shell thickness around perimeter (285mm below meniscus, 0.04%C, 2.2 m/min)

the plant trial was also measured based on the distance from the billet center to the non-bulged line extended between the two billet off-corner locations (4mm from each edge). These measurements were made on the cold section and varied greatly from 0 to over 2mm. Considering the uncertainties when evaluating the bulging, the calculated bulging amount seems consistent with the measured value.
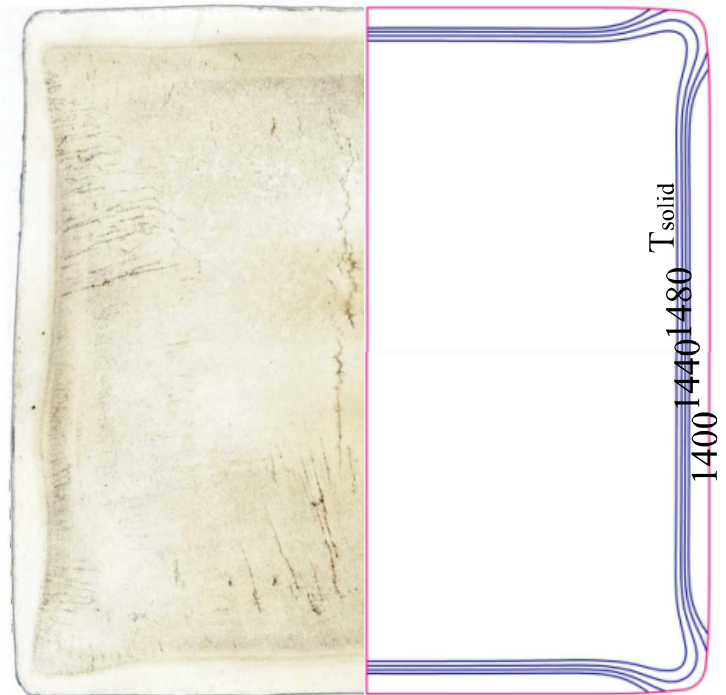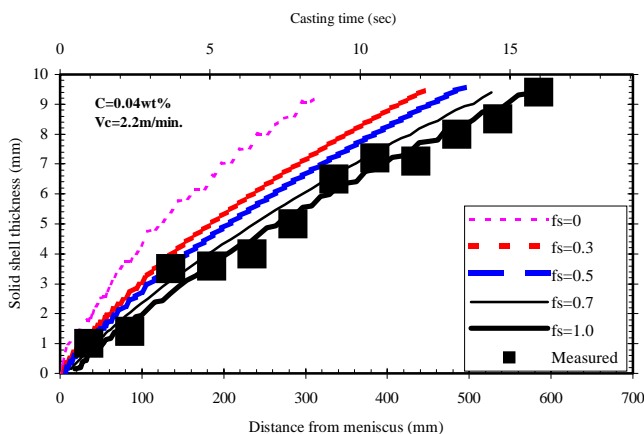

Fig. 8: Comparison of measured and calculated (AMEC2D) shell thickness growth down mold
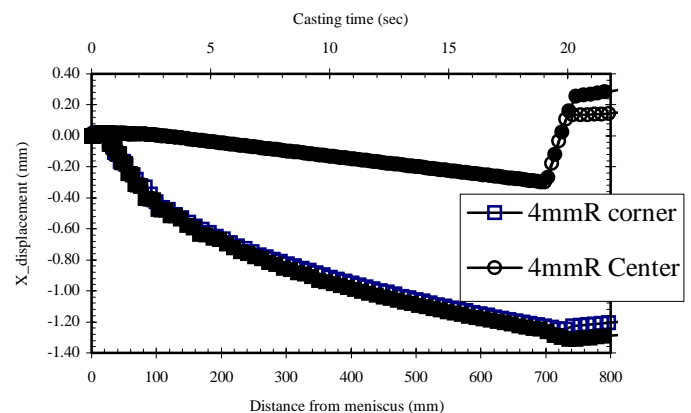

Fig. 9: Evolution of billet surface displacement showing center bulging just below mold exit

Stress and Crack Prediction - Stress profiles within the solidifying shell are generally compressive on the surface and tensile in the interior, as in Fig. 4(b). The curve shapes change due to the sudden increase in

strength in transforming from delta to austenite. There are also variations around the perimeter, due to local stress concentration effects near the corner regions. Although the stress predictions could not be verified, billet samples were obtained under various casting conditions and their microstructures evaluated. Of particular interest is the location of cracks relative to the model predictions.
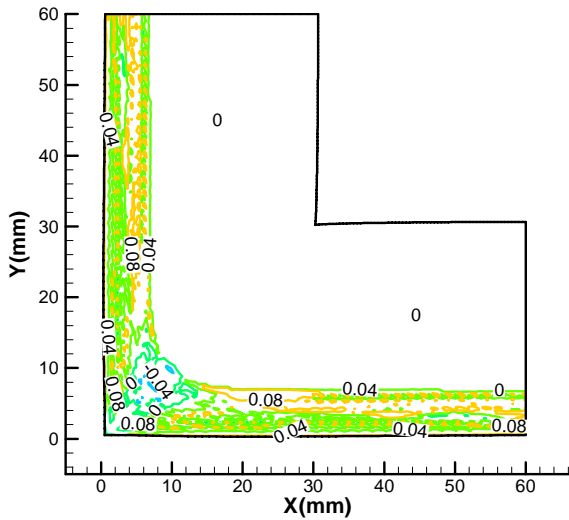
(a) Damage strain, at mold exit
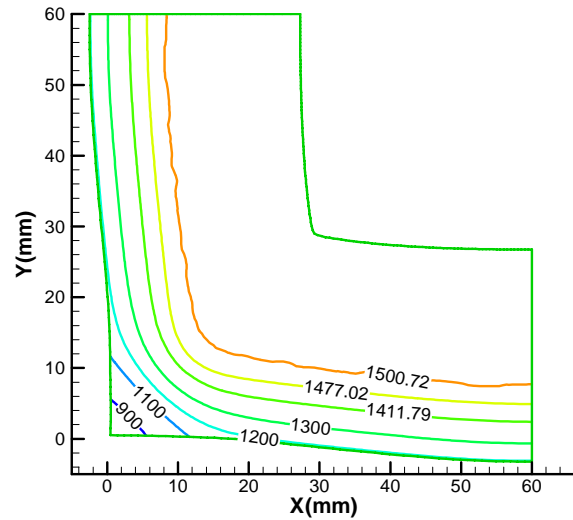
(c) Distorted temperature contours, 200mm below mold exit
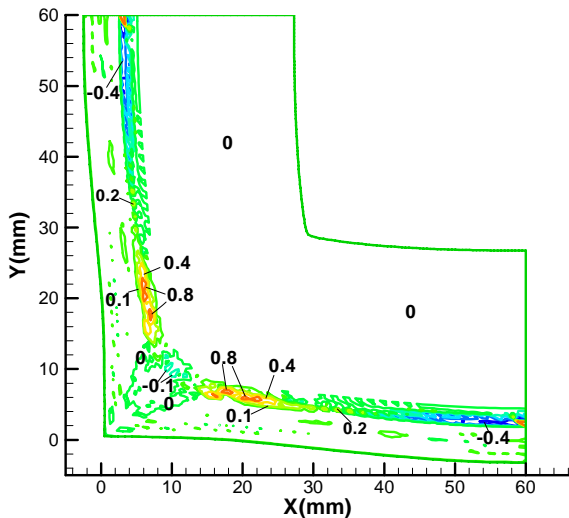
(b) Damage strain, 200mm below mold exit

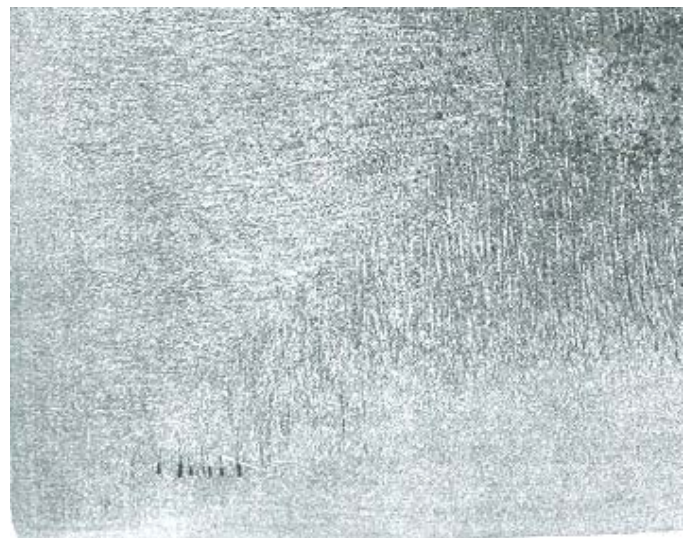Fig. 10: Model results (CON2D: 0.27%C, 5.0m/min, perfect taper)

Fig. 11: Macro-etched section through billet showing off-corner subsurface longitudinal cracks

Surface cracks were not generally found for the conditions of the plant trial, casting at only 2.2 m/min. This matches model predictions that the maximum damage strain was only 0.08%, relative to a critical strain of 0.4%, for these conditions.[11] Increasing the casting speed to 5 m/min, however, causes the damage strain to increase, due to the hotter and thinner shell being weaker and less resistant to bulging and bending below the mold. Damage strain is predicted to be small at mold exit, Fig. 10(a), but quickly increases below mold exit Fig. 10(b), where the maximum exceeds the critical value of 0.4%, in a small region found 7~8mm beneath the

surface, and 15~23mm from the corner subsurface. This location corresponds to the location of the solidification front, as deduced from the temperature contours in Fig. 10(c). It also matches the position and orientation between dendrites of off-corner subsurface cracks, such as those shown in the macro-etched billet cross section in Fig. 11. Moreover, the critical casting speed of 5 m/min agrees with experimental findings.[19]

RESULTS

Having validated the models, they are applied to understand the mechanism of longitudinal corner cracks and off-corner subsurface cracks, including the effects of corner radius, type of lubrication, taper, and casting speed. The models are then applied to predict the maximum casting speed to avoid crack formation due to bulging below the mold during casting of square steel billets with various section sizes and mold lengths.

This study indicates two distinct mechanisms to generate longitudinal corner cracks or longitudinal off-corner internal cracks in casting steel billets, based on simulations of 120mm square steel billets with 0, 4, and 15mm radius corners.

Longitudinal Corner Cracks: Formation Mechanism

Longitudinal corner cracks are predicted only in the large-corner-radius billet. They form in the mold due to tension within the hotter and thinner shell at the corner. These surface cracks could be driven deeper by solid shell bulging due to mold wear or poor alignment of guide rolls below the mold.

The detailed steps of this cracking mechanism are illustrated in Figs. 12 and 13, which show temperature and stress evolution in the corner region of a billet with 15-mm corner radius. Soon after solidification starts, the shell shrinks away from the corner, due to the inadequate taper of only 0.75%/m. This forms a gap that lowers heat transfer, producing a thinner shell that is also hotter and weaker. Ferrostatic pressure generates tensile hoop stress, which is greatest at the symmetry plane through the corner very near the surface.

The development of hoop plastic strain with time is shown in Fig. 14 at the critical corner location, 1mm deep beneath the corner surface where longitudinal corner cracks were found. This figure reveals that the large corner radius billet develops tensile plastic strain from 4 to 14 seconds in the mold (150 – 520mm below meniscus). This

Fig. 12: Evolution of temperature (AMEC2D: 15-mm corner radius, 2.2 m/min)

is consistent with breakout shell observations that corner cracks begin some distance below the meniscus. Compression is found both before and after this time. Below the mold, bulging makes the shell hinge around the corner, forcing the corner surface into compression, but increasing tensile strain deeper below the subsurface. Thus, corner cracks initiating in the mold may grow more severe below the mold, producing the severe defects shown in Fig. 1(a). This detrimental bulging may occur both in the mold, due to mold wear, or below, due to poor alignment of guide rolls.
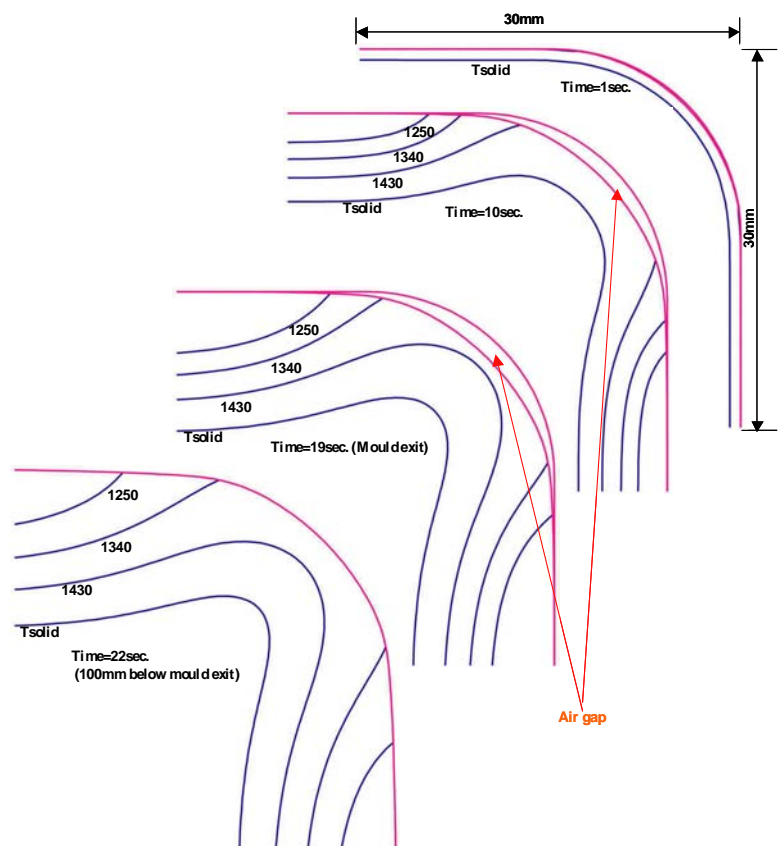
The small radius billet experiences compression at the corner throughout casting (see Fig. 14) owing to two-dimensional cooling at the corner. This finding of higher susceptibility to corner surface cracks with large corner radius matches well with plant observations.[3, 31] It is also noted from Fig. 14 that using mold powder as a lubricant lowers the strain and crack sensitivity, due to formation of a more uniform shell.
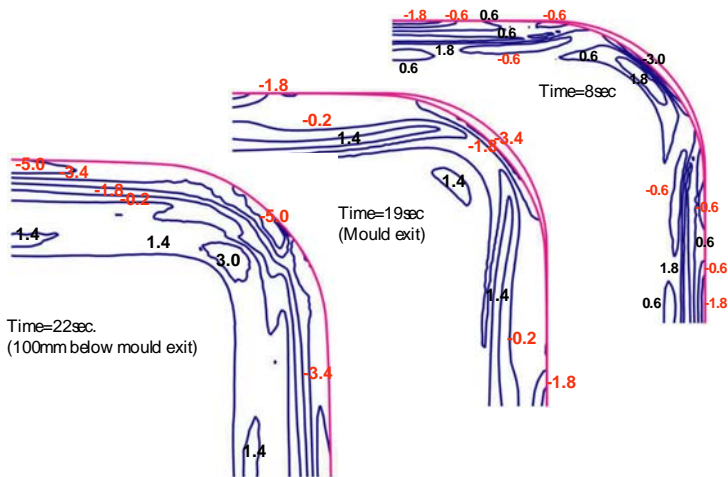

Fig. 13: Evolution of stress contours (AMEC2D: 15-mm corner radius; 2.2 m/min)
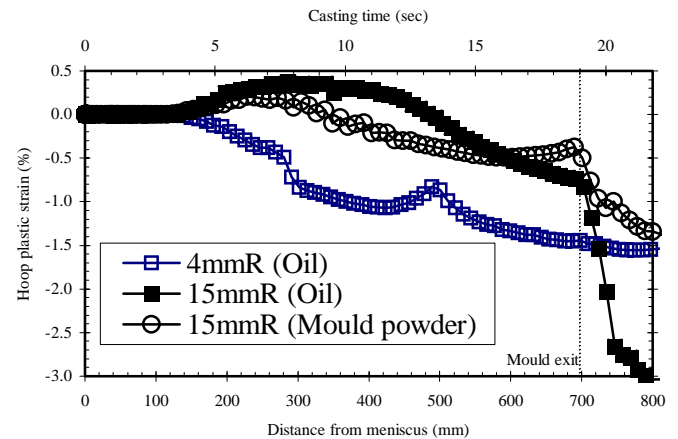

Fig. 14: Evolution of hoop plastic strain, at 1mm below billet corner surface

Longitudinal Off-Corner Subsurface Cracks: Formation Mechanism

Longitudinal off-corner subsurface cracks are predicted to form more easily in small-corner-radius billets. They are caused by hinging of the thin, weak shell around the corner at the off-corner region, due to bulging allowed either in the mold by mold wear, or below the mold by poor guide-roll alignment.

The important steps in the mechanism are modeled in Fig. 10.   For small-corner radius billets, stress in the mold is relatively low, and the surface is in compression. The shell in the off-corner region is thin and weak if the taper is only 0.75%/m, due to the off-corner gap. With ideal taper, the shell thickness is relatively uniform, as shown in Fig. 10(c). The corner in either case is slightly thicker, owing to 2-D heat conduction.

Below the mold, ferrostatic pressure is able to push the billet faces outward, as shown in Figs. 10(b) and 10(c). This causes the shell to bend around the corner, particularly at the off-corner region. This generates tensile stress at the inside of the shell within the crack-sensitive mushy region. The stress direction is perpendicular to the dendrite growth direction, so tends to pull apart the interdendritic liquid. The resulting tensile strain increases from only 0-0.1% at mold exit to over 0.4% at 100mm below mold exit. This damage strain causes hot tear cracks at the characteristic off-corner subsurface location observed in Figs. 10(b) and 11. Bending around the corner may also occur inside the mold, if there is excessive mold wear in the lower regions of the mold. The subsurface tensile stress is also worsened by surface reheating, which often occurs after excessive cooling of surface.

Effect of Corner Radius

The shape of the billet corner affects how shrinkage, stress and strain develop there. Figure 15 shows that increasing corner radius increases the size and extent of the interfacial air gap, for the same inadequate taper. The air gap always begins in the corner and grows with time, extending further from the corner. The result is a thinner shell at the corner for the billet with 15-mm corner radius, as compared in Fig. 16 with that for 4-mm radius. Thus, longitudinal corner cracks are predicted to arise only in large corner radius billets, which experience higher tension within the hotter and thinner shell along the exact corner during solidification in the mold.

On the other hand, decreasing corner radius also moves the location of the peak strain from the corner to off-corner. Small corner-radius billets experience higher subsurface bending stresses due to the hinging around the corner that accompanies bulging below the mold. Thus, longitudinal subsurface off-corner cracks are easier. The conclusion is that mold corner radius controls how longitudinal cracks are manifested, but is not the root cause of the problem. This means that large-corner radius molds might be used effectively to improve smooth rolling operations while still maintaining quality billets free of longitudinal cracks, so long as other casting parameters are optimized.

Effect of Lubrication Type

Changing from oil to mold powder lubrication both decreases overall heat flux and makes heat transfer more uniform around the billet perimeter. These effects are illustrated in Fig. 16. The thicker mold slag layer causes lower heat flux, leading to a hotter and thinner steel shell on average. The gap at the corner is smaller, due mainly to less shrinkage of the hotter shell. The ability of mold slag to flow into gaps, and its higher conductivity relative to gas-filled gaps, also contributes. This increased uniformity is beneficial for crack prevention. In oil casting, this extra uniformity could be achieved by increasing taper.

Changing the lubricant from oil to powder does not change the nature of the stress and strain development or susceptibility of large and small corner radius billets
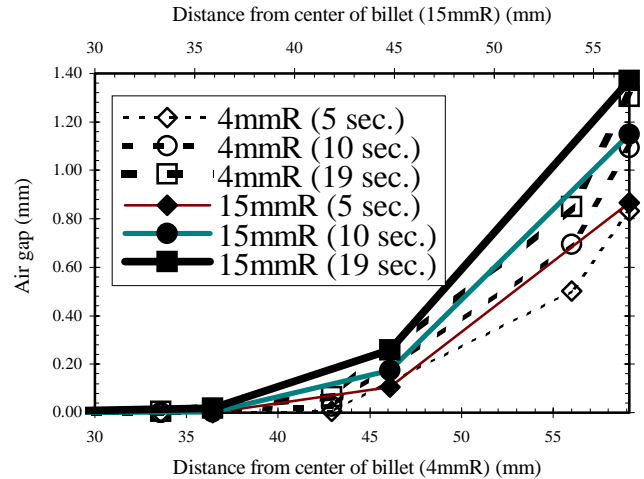

Fig. 15: Effect of mold corner radius on corner gap size evolution

to corner and off-corner cracks, respectively. With mold powder, the heat flux is lower and the solidifying shell is hotter and weaker. Thus, despite the increased uniformity around the billet perimeter, all of the stresses and strains, and the associated longitudinal cracks are slightly worse.

Effect of Mold Taper

Heat transfer in the mold corner region, which governs the growth and temperature of the shell there, is controlled by the size of the interfacial gap. This is influenced by the mold taper, relative to shrinkage of the strand cross section. The effect of taper on axial profiles of surface temperature at the strand center and corner is shown in Fig. 17. Regardless of taper, the centerline surface temperature has the same profile, decreasing monotonically to 900 °C at mold exit. This is because the billet strand is always in good contact with the mold at the strand center. The temperature rebound below the mold is simply due to the slower rate of heat removal by the sprays.

At the corner, the temperature rebounds after about 1 second for both tapers due to air gap formation. This time corresponds to initial formation of the air gap and is delayed by applying the taper (b). An air gap still forms because the linear taper of 0.75%/m is not
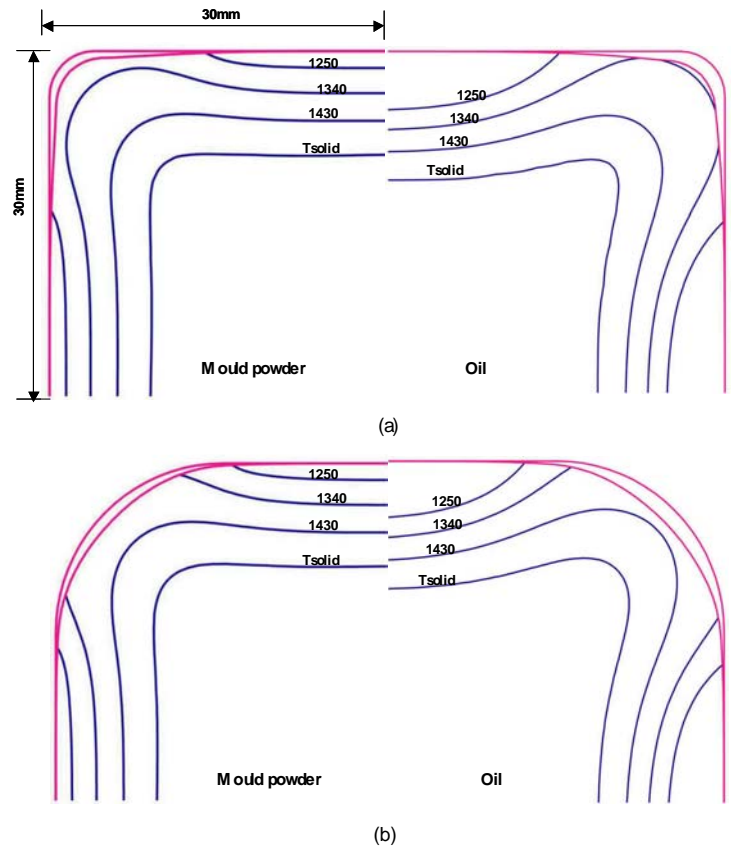

Fig. 16: Effect of mold corner radius and lubricant on temperature contours and shell thickness (mold exit) (a) 4-mm corner radius (b) 15-mm corner radius

sufficient to match the shrinkage of the shell. The corner gap persists throughout casting, keeping the temperature there much higher than at the center. This enhances hinging below the mold, which exacerbates longitudinal cracks.
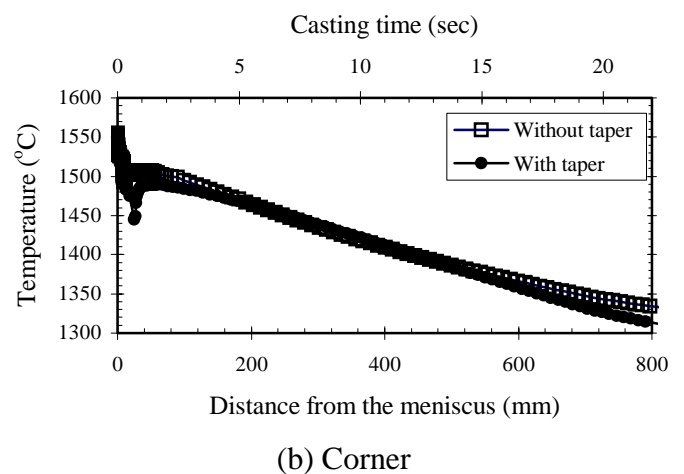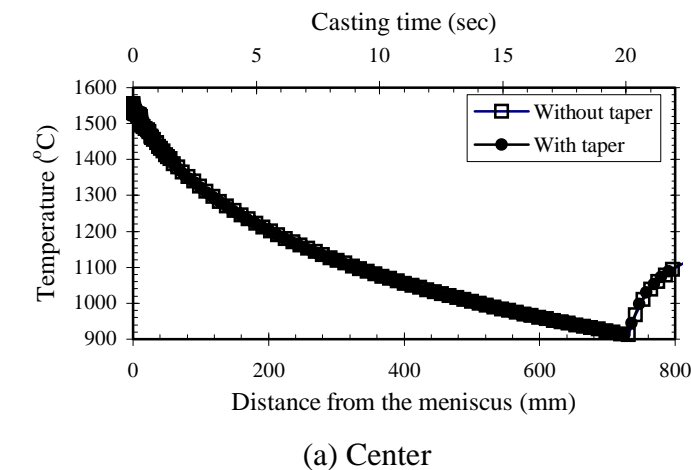

(a) Center

(b) Corner

Fig. 17: Effect of mold taper on surface temperature along strand (4-mm corner radius)

Employing an optimized parabolic mold taper would improve uniformity of shell growth around the mold perimeter. This could make the shell corners colder than the center, rather than hotter. This would improve resistance to off-corner subsurface longitudinal cracks, in the same manner as mold flux, except that overall

heat flux would not suffer. This would allow a greater casting speed without cracking, other factors remaining the same.

Mold wear effectively lowers the taper and likely worsens both types of longitudinal cracking problems. Mold wear at the corner would cause a more severe gap, leading to a hotter and thinner shell there, which would increase the susceptibility to corner surface cracks. Mold wear at the center would allow billet bulging to occur inside the mold. This could allow the hinge action inside the mold, and increase the susceptibility to off-corner subsurface cracks. Permanent distortion of soft copper mold tubes would have a similar detrimental effect. Misaligned or missing guide rolls also aggravate the below-mold bulging and hinging mechanism.

Critical Casting Speed

Increasing casting speed shortens time in the mold, resulting in a thinner, weaker shell that is more susceptible to longitudinal cracks, especially due to increased bulging just below mold exit. The results in Fig. 10 show for the typical case of a 120mm section size and 800mm mold length, that subsurface, off-corner longitudinal cracks are expected when the casting speed exceeds 5.0 m/min. Further simulations were performed to predict this critical casting speed as a function of section size and working mold length (distance from meniscus to mold exit). Conditions were the same as the plant validation case, Table 3, except for changing the steel grade (see Table 2), decreasing the pour temperature to 1540 ^{o}C, and employing ideal taper which caused uniform heat flux around the strand perimeter. The heat flux profile is included in Figs. 3 and 6.

As expected, higher casting speed leads to higher plastic strain at the off-corner sub-surface region as well as greater bulging just below mold exit, as indicated by Fig. 18. With increasing distance below mold exit, sub-mold bulging eventually plateaus due to the shell growth. The increase in maximum bulging with casting speed is revealed in Fig. 19. For a given section size, bulging increases sharply as casting speed increases near the critical casting speed indicated by hot tear criterion. This sharp threshold suggests that the critical casting speed may not be particularly sensitive to steel grade.

Figure 19 could be used to determine casting speed limit under any specific maximum bulging criterion. Off- corner sub-surface longitudinal cracks form when the maximum bulging reaches 4 to 10mm. The critical speeds to avoid cracks, thus, are higher than the critical speeds to satisfy the 1mm maximum bulging criterion, given the same section size and mold length.
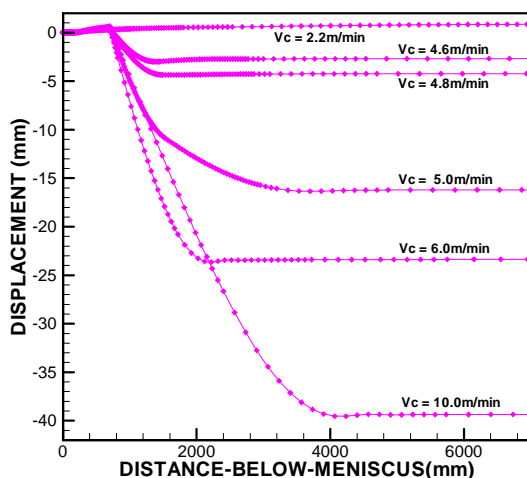

Fig. 18: Effect of casting speed on displacement histories along surface center (120mm section, 700mm working mold length)
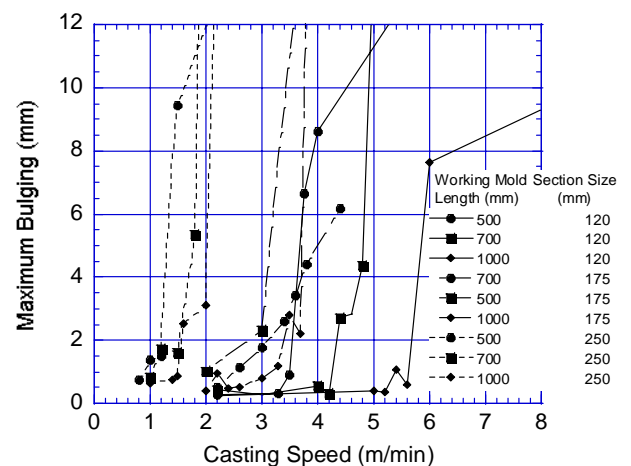

Fig. 19: Effect of casting speed on maximum centerline bulging

Effect of Section Size and Mold Length

Figures 20 and 21 present the critical casting speed for different section sizes and working mold lengths, based on the hot tear criterion and the 1mm maximum bulging criterion, respectively. The critical casting speed increases as the working mold length increases for a given section size. For example, the critical casting speed based on the cracking criterion increases from 3.75m/min. to 6m/min. as the working mold length increases from 500mm to 1000mm for 120mm square section size. This is due to colder and thicker shell at mold exit for the longer dwell time in the mold.
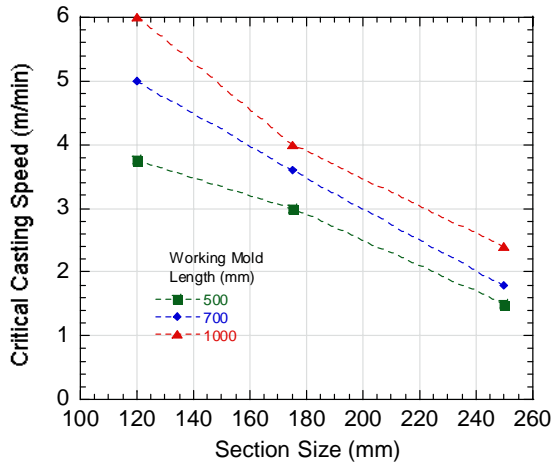

Fig. 20: Critical casting speeds, based on criterion to avoid off-corner longitudinal cracks
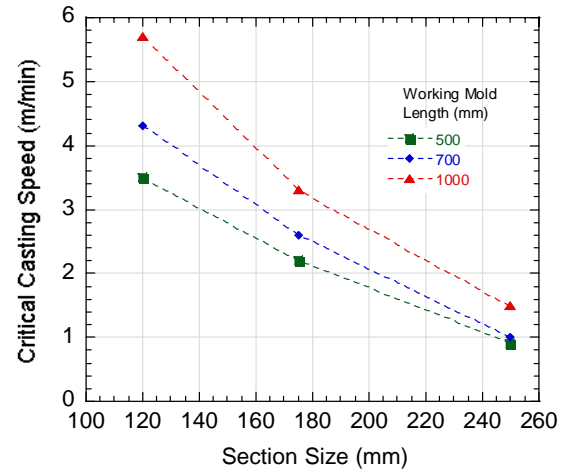

Fig. 21: Critical casting speeds, based on criterion to avoid 1-mm maximum center bulge

The critical speed decreases as the section size increases in a given mold length. For example, the critical casting speed based on the cracking criterion decreases from 5m/min. to 1.8m/min. as the section size increases from 120mm to 250mm for 800mm mold. It is very sensitive to the mold section size because the larger surface subjected to ferrostatic pressure provides a lever arm for much bending around the corner.

Note that the critical casting speeds in the larger section size mold, 250mm×250mm, were underestimated in this study. This error is due to neglecting the axial support provided by mold bottom, which is not included in the 2D model. Thus the critical casting speed predictions in this work are expected to be slightly conservative.

RECOMMENDATIONS

- Many considerations govern casting speed limits to produce high quality steel billets. These include ensuring that the metallurgical length is before torch cutoff, that the surface does not reheat excessively after exiting the spray zones, that mold oscillation produces negative strip, that a variety of cracking problems are avoided, and a number of other considerations. The rate-limiting problem should be determined for each given steel plant.

- Decreasing mold corner radius to 4-6mm is effective at preventing longitudinal corner cracks. Care must be taken, however, to avoid replacing them with off-corner subsurface longitudinal cracks.

- Casting speed should be restricted according to section size, mold length, and heat transfer conditions, in order to avoid longitudinal cracks. A figure such as Fig. 21 is a tool for mold designers or operators to determine critical casting speeds for any chosen maximum bulging criterion. For the conditions assumed here, critical casting speeds of 5 m/min (120mm square section and 800mm mold) and 1.5 m/min (250mm square section and 500mm mold) are predicted.

- Maximum casting speed must decrease with increasing section size, due to the higher off-corner subsurface tensile strain caused by larger ferrostatic bending force below mold exit. Thus, increasing section size produces less productivity increase than expected. For the conditions assumed here,

increasing section size from 120mm to 250mm for a 800mm mold, decreases the critical casting speed from 5.0m/min. to 1.8m/min. This increases productivity only 50% from 0.6 tonne/min to 0.9 tonne/min.

- Increasing mold length allows higher maximum casting speed and increased productivity, due to the colder, thicker, and stronger shell at mold exit. For the conditions assumed here, increasing mold length from 600mm to 1100mm for a 120mm section, increases the critical casting speed from 3.75 m/min. to 6m/min.
- Properly aligned, well-maintained foot rolls should be used to guide and support the strand below the mold. This should allow significant increase in casting speed and productivity without off-corner longitudinal cracks. This approach has the advantage over increasing mold length, in that surface temperature can be easily controlled by sprays and the shorter mold is less sensitive to mold taper problems. More study is needed to quantify the increase for different section sizes and mold lengths.
- Mold tubes of creep-resistant copper should be employed to minimize permanent mold distortion together with frequent mold inspection and maintenance to keep worn molds out of service, in order to avoid bulging in the mold and the accompanying longitudinal cracks.
- An optimized parabolic mold taper should be employed that matches shrinkage of the shell, in order to encourage uniform heat transfer around the billet perimeter, and to discourage mold wear.
- Changing from oil lubrication to powder casting leads to a more uniform shell in the mold, which is generally beneficial. However, this also lowers mold heat transfer, so less taper is needed and the maximum casting speed may have to be lowered to avoid longitudinal cracks.
- If the above recommendations are followed, then large corner radius billets should be castable without longitudinal cracks, with the benefit of a smoother corner for rolling operations.

SUMMARY

Computational models of continuous casting of steel in square billet molds are validated with measurements and applied to investigate temperature, shrinkage, stress, and longitudinal cracks in the shell. For conventional taper, increasing corner radius increases longitudinal surface corner crack formation in the mold. Flux lubrication helps by increasing uniformity. Increasing casting speed or section size or shortening mold length increases off-corner subsurface longitudinal cracks, as bulging causes hinging around the corner, especially below mold exit with no foot rolls. Longitudinal crack formation mechanisms are quantified in this work and guidelines are presented to avoid them, based on critical casting speed limits which depend on section size, mold length, and other parameters.

ACKNOWLEDGEMENTS

REFERENCES

1. I.V. Samarasekera, J.K. Brimecombe and K. Wilder, "The Pursuit of Steel Billet Quality," Ironmaking and Steelmaking, Vol. March, 1994, 53-63.

2. R. Hauri, "Continuous Casting Moulds: Design, Material, Coating," Advances in Continuous Casting: Research and Technology, (Cairo, Egypt), Woodhead Publishing Ltd., UK, 1992, 291-298.

3. Y. Aketa and K. Ushijima, Tetsu to Hagane Overseas (J. Iron Steel Inst. Jpn), Vol. 2 (4), 1962, 334-343.

4. I.V. Samarasekera and J.K. Brimecombe, "The Influence of Mold Behavior on the Production of Continuously Cast Steel Billets," Metallurgical Transactions B, Vol. 13B (1), 1982, 105-116.

5. V.P. Perminov, N.M. Lapotyshkin, V.E. Girskii, A.I. Chizhikov, "Prevention of Distortion in A Continuously-Cast Square Alloy Steel Billet," Stal. in English, Vol. 7, 1968, 560-563.

6. H. Mori, "Causes and Prevention of Defects in Continuous Casting. Pt. 1," Tetsu-to-Hagane (J. Iron Steel Inst. Jpn.), Vol. 58 (10), 1972, 1511-1525.

7. W.P. Young and W.T. Whitfield, "Casting of Quality Steel at Wisconsin Steel," 51ST National Open Hearth and Basic Oxygen Steel Conference, AIME, NEW YORK, Vol. 51, 1968, 127-132.

8. K. Matsunaga, Y. Ohkita, S. Hirayama, S. Kimiya, S. Kojima, "Progress in the Continuous-Strand Casting of Billets at Kokura Steel Works of Sumitomo Metals. (Retroactive Coverage)," 59th National Open Hearth and Basic Oxygen Steel Conference, (St. Louis, Mo.), Metallurgical Society AIME, New York, N.Y., 1976, 228-249.

9. Y. Aketa and K. Ushijima, Tetsu-to-Hagane (J. Iron Steel Inst. Jpn.), Vol. 45, 1959, 1314-1345.

10. J.K. Brimacombe, F. Weinberg and E.B. Hawbolt, "Formation of Longitudinal, Midface Cracks in Continuously-Cast Slabs," Can. Met. Quart., Vol. 19, 1980, 215-227.

11. C. Li and B.G. Thomas, "Maximum Casting Speed for Continuous Cast Steel Billets Based on Sub-mold Bulging Computation," 85th Steelmaking Conference, (Nashiville, TN), ISS-AIME, Warrendale, PA, Vol. 85, 2002, 109-130.

12. C. Chow, Master Thesis Thesis, The University of British Columbia, 2001.

13. AMEC2D, AMEC2D Manual, Seoul National University, Seoul, Korea, 1996.

14. J.K. Park, B.G. Thomas and I.V. Samarasekera, "Analysis of Thermal-Mechanical Behavior in Billet Casting with Different Mould Corner Radii," Ironmaking and Steelmaking, in press,

15. H. Zhu, "Coupled Thermal-Mechanical Finite-Element Model with Application to Initial Solidification," Ph.D. Thesis, University of Illinois at Urbana-Champaign, 1996.

16. A. Moitra, "Thermo-Mechanical Model of Steel Shell Behavior in Continuous Slab Casting," Ph.D. Thesis, University of Illinois at Urbana-Champaign, 1993.

17. E. Lemmon, "Multi-dimentional Integral Phase Change Approximations for Finite-Element Conduction Codes," in Numerical Methods in Heat Transfer, Vol. 1, R.W. Lewis, K. Morgan and O.C. Zienkiewicz, eds., John Wiley & Sons, 1981, 201-213.

18. Y.M. Won and B.G. Thomas, "Simple Model of Microsegregation during Solidification of Steels," Metallurgical and Materials Transactions A, Vol. 32A (July, 2001), 2001, 1755-1767.

19. D. Lorento. Personal Communication. (2001),

20. C. Li and B.G. Thomas, "Analysis of the Potential Productivity of Continuous Cast Molds," Brimacombe Memorial Symposium, (Vancouver, Canada), Canadian Inst. Min. Metall., 2000, 17, 201.

21. M.M. Wolf, "Mold Length in Slab Casting - A Review," Ironmaking and Steelmaking, Vol. 23 (2), 1996, 47-51.

22. J.K. Park, I.V. Samarasekera, B.G. Thomas, U.S. Yoon, "Analysis of Thermal and Mechanical Behavior of Copper Mould During Thin Slab Casting," 83th Steelmaking Conference Proceedings, (Pittsburgh, PA), Iron and Steel Society, Vol. 83, 2000, 9-21, 061.

23. N. Kapaj, M. Pavlicevic and A. Poloni, "Exceeding the casting speed of bloom CC machines by three times," 84th Steelmaking Conference, (Baltimore, MD), Iron and Steel Society/AIME, Warrendale, PA, Vol. 84, 2001, 67-78, 222.

24. J.K. Brimacombe, "Design of continuous casting machines based on a heat-flow analysis: state-of-the-art review," Canadian Metallurgical Quarterly, Vol. 15 (2), 1976, 163-175.

25. C. Li and B.G. Thomas, "Thermo-Mechanical Finite Element Model of Shell Behavior in the Continuous Casting of Steel," J. Key Engineering Materials, Australia, 2002, 7p, in press.

26. Y. Won, T.-J. Yeo, D. Seol, K. Oh, "A New Criterion for Internal Crack Formation in Continuously Cast Steels," Metallurgical and Materials Transactions B, Vol. 31B (4), 2000, 779~794.

27. J.H. Weiner and B.A. Boley, "Elasto-Plastic Thermal Stresses in A Solidifying Body," J. Mech. Phys. Solids, Vol. 11, 1963, 145-154.

28. Wang, B.N. Walker and I.V. Samarasekera, Can. Met. Quart., Vol. 39 (4), 2000, 441-454.

29. J. Fu, Master Thesis Thesis, The University of British Columbia, 2001.

30. C.A.M. Pinheiro, I.V. Samarasekera and B.N. Walker, "Mould heat transfer and continously cast billet quality with mould flux lubrication," Ironmaking and Steelmaking (UK), Vol. 27 (1), 2000, 37-54.

31. Y. Aketa and K. Ushijima, Tetsu-to-Hagane (J. Iron Steel Inst. Jpn.), Vol. 46, 1960, 1733-1740.